New electrochemical reactor design for emergent pollutants removal by electrochemical oxidation

Renato Montenegro-Ayo[a,b,c], Tzayam Pérez[d], Marcos R.V. Lanza[e], Enric Brillas[f], Sergi Garcia-Segura[a,*], Alexsandro J. dos Santos[a,e,*]

[a] *School of Sustainable Engineering and the Built Environment, Arizona State University, Tempe, Arizona 85287-3005, United States*

[b] *Centro de investigación y Desarrollo Tecnológico Industrial (CIDTI), ANALYZEN PERU S.A.C., Mz. S. Lt. 1 Asociación Villa la Paz de Jicamarca, Huarochirí, Anexo 22, Lima, Perú*

[c] *Departamento de investigación y desarrollo tecnológico de aguas residuales (DIDAR), LIMAEM S.A.C., Morro Solar 230, dpto. 1002, Santiago de Surco, Lima, Perú*

[d] *Departamento de Ing, Química, DCNE, Universidad de Guanajuato, Noria Alta s/n, NoriaAlta, Guanajuato C.P. 36050, Mexico*

[e] *São Carlos Institute of Chemistry, University of São Paulo, Avyenida Trabalhador São-Carlense 400, São Carlos, SP, 13566-590, Brazil*

[f] *Laboratori d'Electroquímica dels Materials i del Medi Ambient, Secció de Química Física, Facultat de Química, Universitat de Barcelona, Martí i Franquès 1-11, 08028 Barcelona, Spain*

Article submitted to be published in Electrochimica Acta

* Corresponding authors:

Alexsandro J. dos Santos - alexsandrojhones@usp.br

Sergi Garcia-Segura – sergio.garcia.segura@asu.edu

Abstract

This paper presents the theoretical and experimental confirmation of the performance of a novel pre-pilot reactor design implementing a boron-doped diamond (BDD) anode to destroy emerging pollutants by electrochemical oxidation. Turbulent flow simulation and secondary current distribution modeling with a COMSOL Multiphysics software were used to assess the engineering capabilities of the reactor along with the oxidant BDD(•OH) electrogeneration at the anode. The antibiotic ciprofloxacin (CIP) was chosen as model molecule to assess the oxidation power achieved with the pre-pilot batch plant. In sulfate medium where BDD(•OH) was the main oxidant, faster degradation was determined by increasing current density, CIP content, and pH. The effect of pH was explained by the transformation of the cationic form of CIP in acidic medium into its more easily oxidizable anionic form in alkaline medium. In chloride medium, CIP was more rapidly removed by the faster attack of the generated active chlorine. The degradation was decelerated in carbonate medium by its scavenging effect and in the presence of humic acid by its competitive oxidation with BDD(•OH). The antibiotic abatement also dropped down in tap water and synthetic urine. An almost total mineralization was achieved with a constant energy cost per unit COD mass of 0.6±0.1 kWh $(g\ COD)^{-1}$. The initial N of CIP was pre-eminently converted into nitrate, alongside nitrite and ammonia to lesser extent. Recalcitrant acetic, oxalic, and formic acids were detected as final carboxylic acids.

Keywords: Active chlorine; Ciprofloxacin; COMSOL Multiphysics; Hydroxyl radical; Secondary current distribution model; Wastewater treatment

1. Introduction

Over the past decades, factors such as population growth and rapid urbanization linked to a better quality of life have increased the overuse of antibiotics for the prevention or treatment of bacterial infections [1–3]. Use of antibiotics has as downside the resulting contamination of the aquatic environment when these metabolic active compounds are excreted. The issue of antibiotic pollutions has become a global issue with terrible consequences such as the development of multi-drug resistant bacteria strains [4–6]. Ciprofloxacin (CIP) is a widely used fluoroquinolone antibiotic to treat many bacterial infections. The poor CIP metabolic decomposition results in the excretion of ~80% of the dosed CIP in urine and feces [7]. The widespread use of CIP to treat even minor infections readily treatable with narrower spectrum antibiotics has contributed to decrease CIP efficiency due to the development of bacteria resistance to this antibiotic. In fact, the presence of CIP in water can increase the resistance of genes and bacteria (antimicrobial resistance agents) to not only CIP but also to other related fluoroquinolone antibiotics. Several papers have reported the detection of CIP in wastewater [8–11], groundwater [12–15], surface water [16–18], drinking water [19–22], tap water [23–25] and hospital wastewater [26–30] ranging from concentrations of ng/L to mg/L. The presence of CIP in water may cause adverse effects to human health even at trace concentrations [31–33]. Unfortunately, conventional wastewater treatments are not capable of removing this pollutant because centralized wastewater treatment plants are not built for such purposes. Development of advanced technologies to treat CIP in different water sources including yellow waters is an urgent need to preserve antimicrobial activity and protect the environment.

Technologies that use electricity to treat contaminated water known as electrochemical advanced oxidative processes (EAOPs) have recently highlighted as promising alternative to conventional wastewater treatment methods. The modular and adaptable character of electrified reactors may be an opportunity to advanced decentralized systems to be implemented in hospitals to treat their effluents with a high load of pharmaceuticals [34–36]. Among the different EAOPs, the

electrochemical oxidation (ECO) is the most frequently used process for antibiotics removal due to its simplicity, environmental compatibility, high efficiency, and flexibility to automation and pilot-scale application [37–42]. One of the factors that affect the efficiency of this process is the nature of the anodic material. It is well-known that boron doped-diamond (BDD) anodes can produce oxidizing radicals from water discharge (mainly heterogeneous hydroxyl radical, designed as BDD($^{\bullet}$OH)). The BDD electrocatalysts have been reported to surpass in efficiency Pt and dimensionally stable anodes (DSA) due to their larger electrocatalytic activity (higher overpotential of oxygen evolution with excellent stability) [43–50]. Hydroxyl radical reacts non-selectively with organic contaminants, rapidly leading to their conversion into innocuous by-products or even their total mineralization (i.e., giving CO_2, H_2O, and inorganic ions) [51–55].

In addition to the anode material, the type of the electrolytic reactor plays a significant role in the ECO process [56,57]. Bench reactors treating small solution volumes are usually reported in the literature due to their simplicity that is enough to answer countless scientific questions about the electrochemical mechanisms and the influence of certain operating variables on the removal of target pollutants [58–62]. However, the feasibility of bench reactors in real scenarios has recently been questioned based on often unrealistic extrapolations of data obtained from lab-scale experiments. Too enthusiastic interpretations and assurances could prevent the possibilities of successful large-scale application.

In this work, a new pilot electrochemical batch reactor has been developed to pave the way to clean waters containing emergent pollutants by ECO. Mathematical modeling and simulations were conducted by COMSOL to assess the effectiveness of the designed system. Performance tests with CIP antibiotic as a model pollutant were carried out to confirm its practical application. Experimental variables such as applied current density, pollutant concentration, and initial pH were first tested in a sulfate medium. Then the competitiveness of the system in the treatment of more realistic water samples was evaluated though the treatment of tap water and urine. Generated by-products such as

carboxylic acids and nitrogenated ionic species were identified and quantified. The degradation and mineralization of the pollutant were determined and discussed on the calculated figures of merit.

2. Experimental

2.1 Chemicals

Ciprofloxacin (CIP, CAS: 85721-33-1, 98%, see chemical structure in Fig. 1), sodium sulfate (Na_2SO_4, 99%), sodium chloride (NaCl, 99%), oxalic acid (99%), formic acid (99%), acetic acid (99%), uric acid (99%), humic acid (99%), urea (99%), calcium carbonate (99%), sulfuric acid (H_2SO_4, 96-98%), and acetonitrile (99%) were purchased from Sigma-Aldrich and used without additional purifications. The synthetic solutions were prepared with ultrapure water from Elga Lab Water.

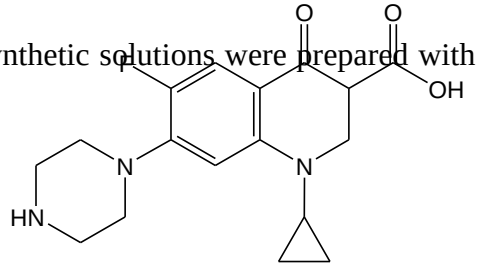

Fig. 1. Chemical structure of ciprofloxacin (CIP).

2.2 Experimental set-up

Electrochemical oxidation was performed at a fixed volume of 2 L using a pre-pilot batch recirculation loop cell containing a BDD anode and a stainless-steel cathode, both of 65 cm^2 of geometrical area. The electrolysis ran at room temperature (25 ºC) and constant current density (*j*) provided by a TENMA model 72–2720 DC power supply. The main experimental variables were *j* (15, 30, 45, and 60 mA cm^{-2}), initial CIP concentration (5, 10, 20, and 30 mg L^{-1}), and initial pH (3.0, 5.0, 7.0, and 10.0) adjusted with a stock solution of 0.5 M sulfuric acid or sodium hydroxide. Synthetic solutions employed 0.050 M Na_2SO_4 as supporting electrolyte. The best operational conditions according to figures of merit observed were selected to evaluate the effect of inorganic ions

commonly present in real effluents (i.e., chloride, carbonate) and natural organic matter using humic acid (HA) as model. Realistic water matrices consisting of tap water and urine were used to evaluate ECO performance. The tap water sample was collected in Tempe AZ /USA and stored at 4 °C. The synthetic urine was prepared with 13.9 mM of urea and 0.10 mM of uric acid. All experiments were performed at similar conductivity of 8-10 mS cm^{-1}.

2.3. Analytical procedure

The concentration of CIP was monitored over time using a Waters HPLC system model e2695, equipped with a C-18 column (75 mm × 4.6 mm, 3.5 µm) coupled to a PDA detector (at 275 nm). Samples of 10 µL were injected into the LC and the mobile phase consisted of an 80:20 mixture of ultrapure water acidified with 0.1% acetic acid and acetonitrile pumped at a flow rate of 0.3 mL min^{-1}. A defined peak for CIP was displayed in the chromatograms at a retention time of 3.91 min. The percentage of CIP removal was then calculated as follows:

$$\%\ \text{CIP removal} = \frac{\text{CIP}_0 - \text{CIP}}{\text{CIP}_0} \times 100 \quad (1)$$

where CIP_0 and CIP are the concentration at initial time and time *t*, respectively. The concentration decays obeyed a pseudo-first order kinetics, allowing to determine the apparent rate constant k_1 (in min^{-1}) from Eq. (2):

$$\ln\left(\frac{\text{CIP}_0}{\text{CIP}}\right) = k_1\, t \quad (2)$$

The chemical oxygen demand (COD) was determined using low range COD kits from Hach. Volume of sample required for analysis was placed in the vials and digested for 120 min at 150 °C using a Hach model DRB200 digester. Thereafter, COD was measured using a Hach UV-vis spectrophotometer DR 6000. The average current efficiency (ACE) and the energy consumption per unit COD mass (EC_{COD}) were calculated from the determined COD values using Eq. (3) and (4), respectively [63]:

$$\mathrm{ACE} = \frac{F\,V\,(\mathrm{COD}_0 - \mathrm{COD}_t)}{8\,I\,t} \quad (3)$$

$$\mathrm{EC_{COD}(kWh\ (g\ COD)^{-1}) = \frac{E_{cell}\,I\,t}{V\,(COD_0 - COD)}} \quad (4)$$

where COD_0 and COD_t correspond to the chemical oxygen demand at the beginning of the treatment and a time *t*, respectively (g O_2 L^{-1}), *F* is the Faraday constant (96,487 C mol^{-1}), *V* is the volume of solution (L), 8 is the oxygen equivalent mass (g eq^{-1}), *I* is the applied current (A), *t* is the electrolysis time in s for % ACE and in h for EC, and E_{cell} is the average potential difference between the electrodes in the cell (V).Duplicate trials for concentration and COD decays were made and average values are reported with a 95% confidence interval.

Generated carboxylic acids were identified by injecting 20 μL of the sample into a Waters HPLC system equipped with Bio-Rad Ion Exclusion Column Aminex HPX-87H (300 mm × 7.8 mm) at 35 ºC. The detection was accomplished at 210 nm in a 2998 PDA detector. The mobile phase contained 0.004 M H_2SO_4 being pumped at a flow rate of 0.6 mL min^{-1}. The retention times were 6.11, 13.05 and 14.28 min for oxalic, formic, and acetic acids, respectively. Nitrogenated, chloride and free chloride species were detected using Hach analytic kits.

2.4. Formulation of the numerical simulation of the electrochemical cell

2.4.1. Pre-pilot batch recirculation cell

The electrochemical system used in the experiments of CIP degradation by ECO was simplified to stablish the simulation domain and it is represented in Fig. 2. The reactor consisted of a BDD circular disc of 10 cm diameter at the bottom, and a concave stainless steel disc cathode of 5.5 cm diameter with a hole in the middle, connected with a pipe of 33.3 cm length and 0.66 cm internal diameter. The overall volume was of 2000 cm^3 and the interelectrode gap of 2 cm. The solution was recirculated at 8 L min^{-1}. Here, theoretical fluid flow and current distribution models were implemented to evaluate the performance in terms of momentum and charge transfer. Mathematical modeling and simulations were implemented with software COMSOL Multiphysics® by solving

governing equations through finite element method. Table 1 summarizes the kinetic parameters and the solution properties that were considered for the model simulations. Mass and charge balances were met for all cases. The computational domain consisted of an unstructured mesh with 1135079 elements. Then, the simulation solution was verified by varying the number of elements till converging results remained unchanged around these defined mesh elements. Fluid flow simulations required ~219 min of computational run time and current distribution simulations required ~100 min. The segregate iterative GMRES method was employed to solve for fluid flow equations, while the direct iterative MUMPS method was used to solve for the current distribution. A convergence criterion of $<10^{-5}$ was considered for all the simulations.

2.4.2. Turbulent flow

According to Fig. 2, all inlets and the outlet of the system can cause changes of flow course, rotational flow, and vortex despite low Reynolds numbers. The traditional κ-ε turbulence model was then chosen because it has proved to be very effective to simulate the fluid flow of complex electrochemical systems [64]. In steady state for an incompressible fluid, the governing equations were:

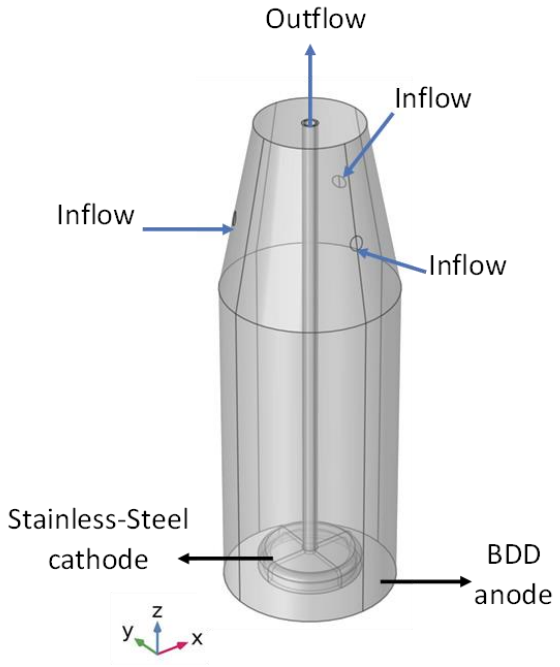

Fig. 2. Simulation domain of the pre-pilot cell used for CIP degradation.

Table 1. Characteristic transport properties and electrochemical kinetic parameters employed in the simulations at 20 ºC.

Dynamic electrolyte viscosity, μ (Pa·s),+	1×10^{-3}
Density of solution, ρ (kg m^{-3}	1000
Inflow velocity, u_0 (m s^{-1})	2.6
Pressure reference, P_0 (Pa)	101325
Conductivity of solution, k (S m^{-1})	0.54
Open circuit potential of the anode, ϕ_{ocp} (V vs SHE) [65]	0.6
Open circuit potential of the cathode, ϕ_{ocp} (V vs SHE) [66]	0.039
Tafel slope of •OH, $b_{\bullet\mathrm{OH}}$ (V dec^{-1}) [65]	0.25
Cathodic Tafel slope, b_c (V dec^{-1}) [66]	0.8
Exchange current density for •OH $j_{0,\bullet\mathrm{OH}}$ (A m^{-2}) [65]	3×10^{-6}
Cathodic exchange current density $j_{0,c}$ (A m^{-2}) [66]	7.5×10^{-3}

$$\rho(\boldsymbol{u}\cdot\nabla\boldsymbol{u}) = -\nabla P + \nabla((\mu+\mu_T)(\nabla\boldsymbol{u} + (\nabla\boldsymbol{u})^{\mathrm{T}}) \quad (5)$$

$$\nabla\boldsymbol{u} = 0 \quad (6)$$

where ρ is the fluid density, $\boldsymbol{u}$ is the average velocity vector, P is the average pressure, and μ the dynamic viscosity. The turbulent viscosity μ_{T} is described by means of Eq. (7) to (9):

$$\mu_{\mathrm{T}} = \rho C_{\mu}\frac{\kappa^2}{\varepsilon} \quad (7)$$

$$\rho(\boldsymbol{u}\cdot\nabla)\kappa = \nabla\cdot\left(\left(\mu+\frac{\mu_{\mathrm{T}}}{\sigma_{\kappa}}\right)\nabla\kappa\right) + P_{\kappa} - \rho\varepsilon \quad (8)$$

$$\rho(\boldsymbol{u}\cdot\nabla)\varepsilon = \nabla\cdot\left(\left(\mu+\frac{\mu_T}{\sigma_\varepsilon}\right)\nabla\varepsilon\right) + C_{\varepsilon1}\frac{\varepsilon}{\kappa}P_\kappa - C_{\varepsilon2}\rho\frac{\varepsilon^2}{\kappa} \quad (9)$$

where κ is the turbulent kinetic energy,ε is the turbulent energy dissipation velocity, and P_κ is an energy production term. The equations use dimensionless model constants C_μ with value 0.09, C_ε with value 1.46, $C_{\varepsilon1}$ with value 1.44, $C_{\varepsilon2}$ with value 1.92, σ_κ equal to1, *and* σ_ε with value 1.3. Details of these parameters have been provided elsewhere [67].

Electrolyte velocities can decrease at the vicinity of the reactor walls, and therefore become dissimilar to the predictions of the turbulent model close to the wall. The Eq. (10) introduces a corrective wall function that is valid for turbulent flow layers [67]:

$$u^+ = 5.5 + \frac{1}{\mathcal{H}}\ln y^+ \quad (10)$$

Where u^+ is defined as dimensionless velocity normal to the wall, $\mathcal{H}$ is the von Karman constant, and the term y^+ is the dimensionless length from the wall to the boundary layer described by Eq. (11):

$$y^+ = \frac{\rho u_\tau y}{\mu} \quad (11)$$

Where u_τ is the friction velocity as estimated from Eq. (12), (,) and y is the distance from the wall [67].

$$u_\tau = C_\mu^{1/4}\sqrt{\kappa} \quad (12)$$

The model is subjected to the following boundary conditions in order to solve Eq. (5)-(9):

- At the electrolyte inlet it is valid the relationship $\boldsymbol{u} = -u_0\boldsymbol{n}$. The term u_0 is defined as the average velocity at the electrolyte inlet and normalized by its product with normal unit vector ($\boldsymbol{n}$). The solution inlet values of κ_0 and ε_0 can be estimated from the turbulent intensity (I_T) fixed at 0.05, and the turbulent length scale (L_T), according to the well-accepted relationships:

$\kappa_0 = 3/2\,(u_0 I_T)^2$ and $\varepsilon_0 = C_\mu^{3/4}\,\kappa^{3/2}/L_T$. The L_T value is determined as $0.07r$ as function of the electrolyte inlet radius r = 0.4 cm.

- At the electrolyte outlet it is considered valid the relationship $[-P + (\mu + \mu_T)(\nabla \boldsymbol{u} + (\nabla \boldsymbol{u})^T)]\boldsymbol{n} = -\boldsymbol{n}P_0$, where P_0 is the pressure at the outlet. Also, $\nabla\varepsilon\cdot\boldsymbol{n} = 0$ and $\nabla\kappa\cdot\cdot\boldsymbol{n} = 0$ at solution exit.
- The local flow velocity u^+ in Eq. (10) was applied to all other boundaries.

2.4.3. Secondary current distribution model

The production of •OH through water oxidation occurs at the interface electrode-electrolyte and this process is limited by charge transfer [68]. Thereby, an analysis of current distribution on the BDD surface could be helpful to evaluate the electrode performance in terms of production of •OH radicals. The secondary current distribution model was themed adequate to analyze this process since boundary conditions only considered surface overpotential through a Tafel kinetics [69]. The governing potential and charge equations given by Laplace's formulation and Ohms law are:

$$\nabla^2\phi = 0 \qquad (13)$$

$$\boldsymbol{j} = -k\nabla\phi \qquad (14)$$

where $\boldsymbol{j}$ is the current density vector, k is the electrolyte conductivity. and ϕ is the electric potential of the solution.

The solution of Eq. (10) and (11) depended on the defined boundary conditions:

- For the BDD anode a charged controlled kinetics was employed, i.e., $j_a = j_{0,\bullet OH} exp\left(\frac{\eta}{b_{\bullet OH}}\right)$, where j_a is the current density at the anode, $j_{0,\bullet OH}$ is the exchange current density, and $b_{\bullet OH}$ is the Tafel constant for hydroxyl radical formation.
- For the stainless-steel cathode, the water reduction kinetic was governed by the expression: $j_c = -j_{0,c} exp\left(\frac{-\eta}{b_c}\right)$, where j_c is the current density at the cathode, $j_{0,c}$ is the exchange current

density, and b_c is the Tafel constant for water reduction.The overpontential is given by $\eta = \phi_M - \phi - \phi_{ocp}$, where ϕ_M is the potential of the metallic electrode and ϕ_{ocp} is the open circuit potential for each electrode.

3. Results and discussion

3.1. Theoretical assessment of the pre-pilot plant

An analysis of the momentum transfer is very important to evaluate the reactor performance in terms of bulk mixing. In this context, Fig. 3a shows the velocity magnitude distribution in a *z*-*y* plane and Fig. 3b presents the flow lines patterns inside the system. The velocity distribution and flow patterns highlighted that the flow entered to the system at 2.6 m s^{-1} and collided with the stainless-steel rod to generate recirculation zones in the middle-body of the reactor. The fluid gets into the concave zone of the cathode and close to the rod hole, thus accelerating due to the drastic decrease of area. Finally, the fluid flow leaves the system with an increment of 0.4 m s^{-1}. Note that recirculation zones are desirable to promote a homogeneous bulk mixing and fluid acceleration is suitable for

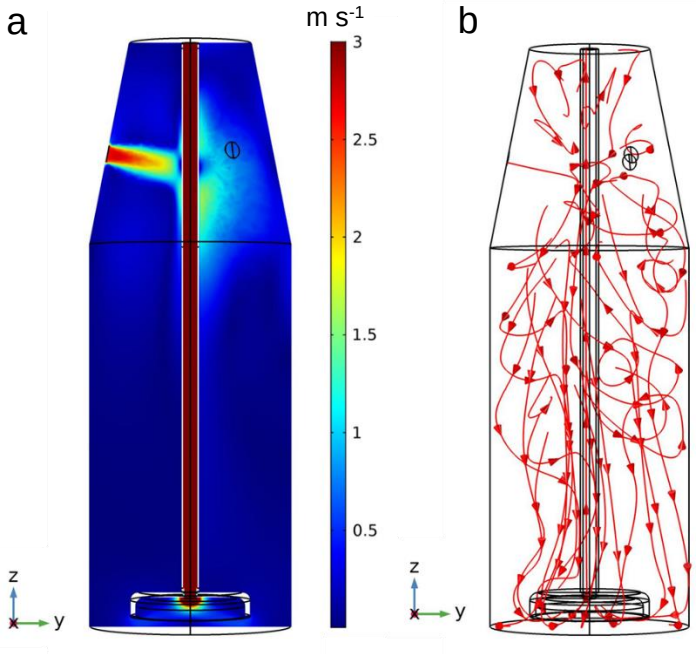

Fig. 3. (a) Velocity magnitude distribution in a *z-y* plane and (b) flow lines patterns inside the proposed electrochemical reactor with u_0 = 2.6 m s^{-1}.

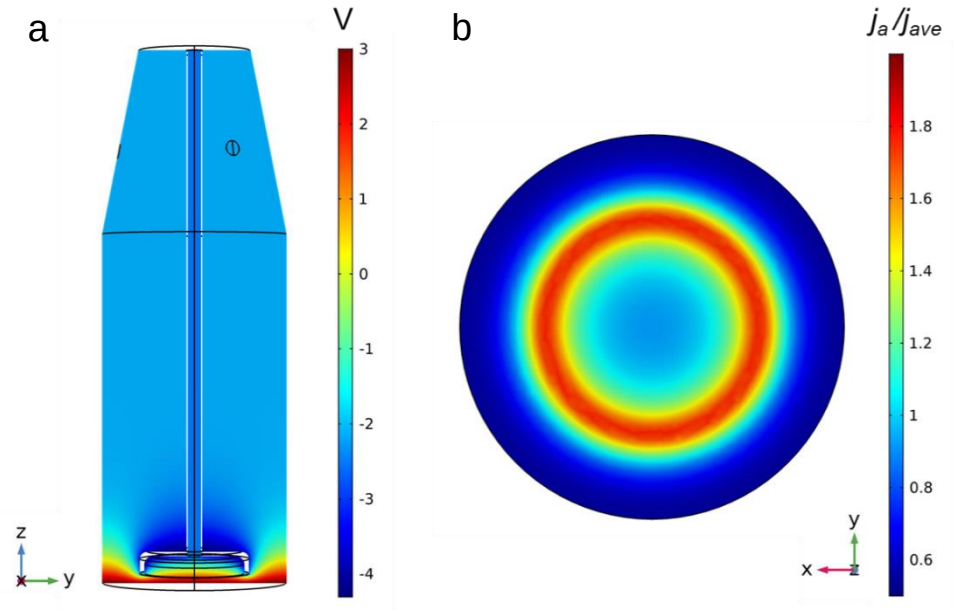

Fig. 4. (a) Potential distribution and (b) normalized current density distribution on the BDD surface of the electrochemical reactor with j_{ave} =25.5 mA cm^{-2}.

minimizing pressure drops. However, next to the BDD electrode the velocity decreased between 0.01 and 0.8 m s^{-1}, which could impact in the mass transfer of the pollutant to the working electrode.

The BDD(•OH) production is very related to the current distribution on the BDD surface, because a non-uniform current distribution could generate zones with more or less quantities of this oxidant and therefore, it may cause an impact in the efficiency of pollutant degradation. Fig. 4a shows the potential distribution and Fig. 4b depicts the normalized current density distribution on the BDD surface of the electrochemical reactor. The potential distribution of Fig 4a follows the geometry and

290 the position of the electrodes, as expected. Meanwhile, Fig. 4b makes evident a non-uniform current
291 distribution generated by the geometry and position of the stainless-steel cathode. A donut of high
292 current was formed at counter position of the cathode, and close to the walls of the reactor, the current
293 decreased. High current zones could promote the undesirable O_2 formation and low current zones
294 could promote the production of lower quantities of BDD(•OH). Nevertheless, the deviation of the
295 normalized current distribution was between 0.6 (60%) to 1.9 (190%), indicating a good performance.
296 One can then infer that the pre-pilot plant could produce an effective amount of BDD(•OH) for the
297 ECO process of CIP, as discussed in the next sub-sections.

298 *3.2. Effect of operating conditions on CIP degradation in sulfate medium*

299 First assays with the novel pre-pilot batch plant with a BDD/stainless steel pair of electrodes
300 were made to assess the effect of *j*, antibiotic concentration, and pH over the performance of CIP
301 degradation aiming to find the best experimental condition for its ECO treatment in sulfate medium.
302 As pointed out above, the main oxidant acting in this process is the physisorbed BDD(•OH), which
303 is formed from the water discharge at the BDD anode from Eq (15) [70–73]. In addition, secondary
304 oxidants such as peroxydisulfate ($S_2O_8^{2-}$, Eq. (16)) and sulfate radical ($SO_4^{\bullet -}$, Eq. (17)) can be
305 electrogenerated in small amounts, slightly contributing to the antibiotic removal [47,74]

306 $$BDD + H_2O \rightarrow BDD(^{\bullet}OH) + H^+ + e^- \quad (15)$$

307 $$SO_4^{2-} + SO_4^{2-} \rightarrow S_2O_8^{2-} + 2e^- \quad (16)$$

308 $$SO_4^{2-} \rightarrow SO_4^{\bullet -} + e^- \quad (17)$$

309 The influence of *j* was studied for 2 L of 10 mg L^{-1} CIP in 0.050 M Na_2SO_4 at pH 7.0 and 25 ºC
310 lasting 300 min. Fig. 5a depicts the gradual rise in the percentage of CIP removal with increasing *j*
311 from 15 to 60 mA cm^{-2}, attaining final values from 84.2% to 99.9% (see Table 2). This behavior can
312 be related to the simultaneous increase in rate of reaction (15) due to the greater E_{cell} achieved (see
313 Table 2), originating higher amounts of BDD(•OH) that more rapidly oxidized the parent molecule.
314 The kinetic analysis of the concentration decays agreed with a pseudo-first order equation and the

corresponding rate constant k_1 with $R^2 > 0.98$ (see Table 2) was calculated from Eq. (2). Fig. 5b shows the progressive increase found for k_1 from 2.3×10^{-3} to 6.3×10^{-3} min^{-1} when passing from 15 to 60 mA cm^{-2}. This presupposes a growth of only 2.74-fold of k_1 for a rise of 4-fold of j. The observed loss of efficiency of the ECO process at higher j can be related to: (i) the parallel oxidation of the by-products formed with BDD($^{\bullet}$OH) and (ii) a larger acceleration of non-oxidizing and parasitic reactions of this radical like O_2 evolution from reaction (18) or $^{\bullet}$OH dimerization to give the weak oxidant H_2O_2 from reaction (19) [47,75,76]:

$$BDD(^{\bullet}OH) \rightarrow BDD + \tfrac{1}{2}O_2 + H^+ + e^- \quad (18)$$

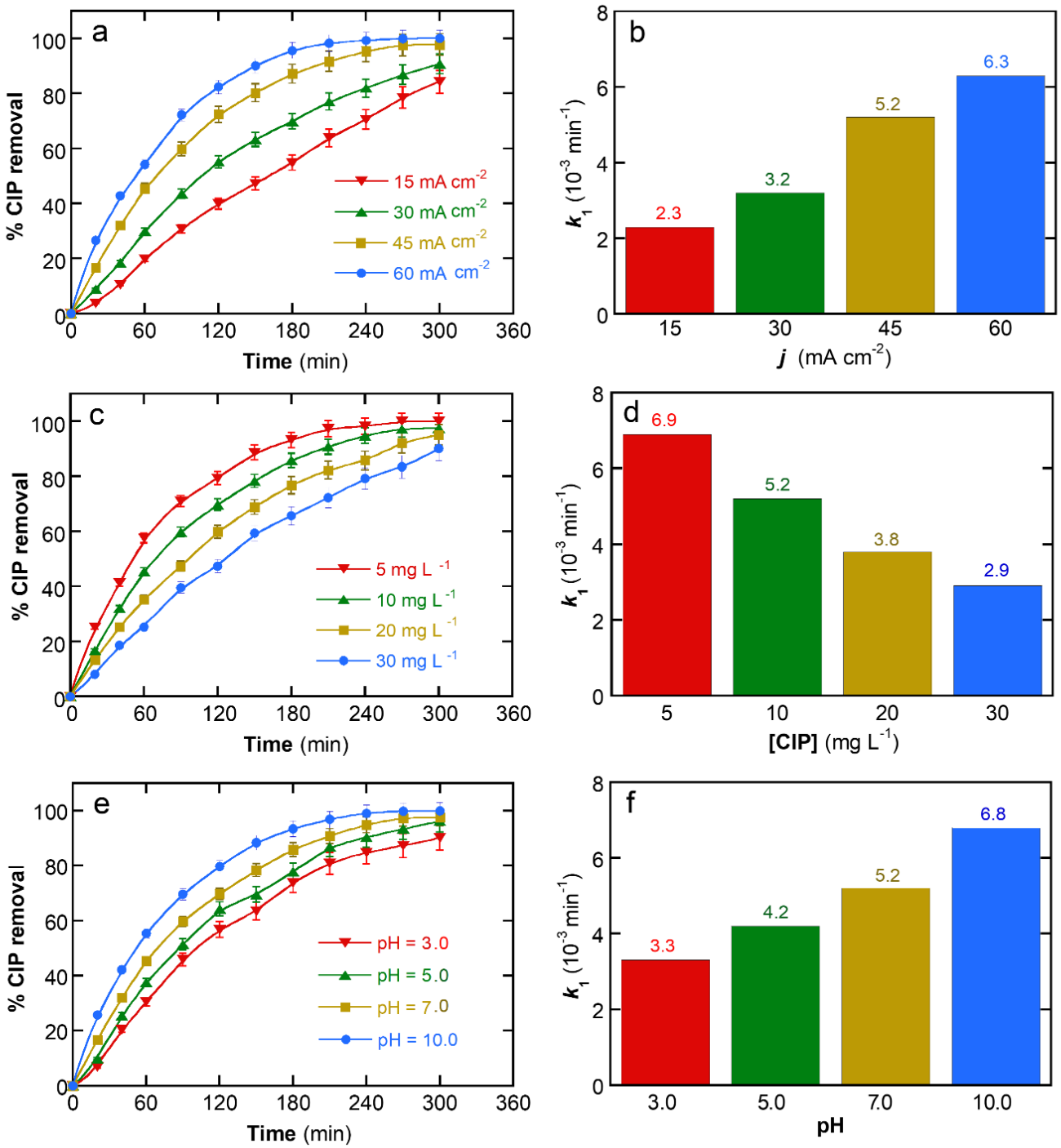

Fig. 5. (a,c,e) Percentage of CIP removal vs. time and (b,d,f) the corresponding pseudo-first-order kinetic analysis for the electrochemical oxidation of 2 L of ciprofloxacin (CIP) solutions in 0.050 M Na_2SO_4 and at 25 ºC using a pre-pilot batch cell with a BDD anode and a stainless-steel cathode, both of 65 cm^2 of geometric area. Effect of: (a,b) j for 10 mg L^{-1} CIP and pH = 7.0, (c,d) initial CIP concentration for j = 45 mA cm^{-2} and pH = 7.0, and (e.f) pH for j = 45 mA cm^{-2} and 10 mg L^{-1} CIP.

329 **Table 2**. Percentage of CIP removal at 300 min, pseudo-first-order rate constant with the
330 corresponding square regression coefficient, and average potential difference of the cell determined
331 for the electrochemical oxidation of 2 L of CIP solutions under different conditions at 25 ºC
332 contained in a pre-pilot batch BDD/stainless-steel cell.

Medium	[CIP] (mg L^{-1})	j (mA cm^{-2})	pH	% CIP removal	k_1 (10^{-3} min^{-1})	R^2	E_{cell} (V)
Control [a]	10	15	7.0	84.2	2.3	0.981	7.3
	10	30	7.0	90.6	3.2	0.995	8.7
	10	45	7.0	97.2	5.2	0.991	9.8
	10	60	7.0	99.9	6.3	0.992	11.2
	5	45	7.0	99.9	6.9	0.991	9.6
	20	45	7.0	95.1	3.8	0.989	9.5
	30	45	7.0	91.3	2.9	0.988	9.6
	10	45	3.0	90.1	3.3	0.997	9.3
	10	45	5.0	96.2	4.2	0.990	9.4
	10	45	10.0	99.9	6.8	0.981	9.8
Cl^- [b]	10	45	7.0	99.9	12.0	0.996	9.4
CO_3^{2-} [b]	10	45	7.0	85.5	3.0	0.997	9.5
HA [c]	10	45	7.0	77.2	2.3	0.994	9.4
Tap	10	45	6.5	95.8	4.4	0.997	9.9
Urine	10	45	7.0	77.2	2.9	0.998	9.3

333 [a] Synthetic solution with 0.050 M Na_2SO_4. [b] Concentration of 5 mM. [c] 5 mM humic acid.
334

$$2BDD(^{\bullet}OH) \rightarrow 2BDD + H_2O_2 \quad (19)$$

Fig. 5c shows that CIP was more slowly degraded when its concentration grew from 5 to 30 mg L^{-1} in 2 L of 0.050 M Na_2SO_4 at pH 7.0, 25 ºC, and j = 45 mA cm^{-2}. The percentage of CIP removal at the end of the runs dropped down from 99.9% to 91.3% (see Table 2) and the expected decay of k_1 from 6.9×10^{-3} to 2.9×10^{-3} min^{-1} is depicted in Fig. 5d. As a first approach, this trend can be interpreted as a decrease of the degradation rate due to the reaction of greater quantities of the antibiotic with a similar amount of generated BDD(•OH). However, while 5 mg L^{-1} of CIP were removed at the lower concentration, a much higher content of 27.39 mg L^{-1} were degraded for 30 mg L^{-1} of CIP. This is indicative of a large enhancement of the oxidation power of the ECO process at higher organic matter, suggesting a faster reaction of CIP with increasing amounts of BDD(•OH) proceeding from the deceleration of its parasitic reactions like reactions (18) and (19).

The effect of pH on the percentage of CIP removal for 2 L of solutions with 10 mg L^{-1} CIP in 0.050 M Na_2SO_4 at 25 ºC and j = 45 mA cm^{-2} is presented in Fig. 5e. A surprising behavior can be observed because the degradation is progressively enhanced from pH 3.0 with 90.1% removal to 10.0 with 99.9% removal (see Table 2). Fig. 5f shows the expected gradual increase in k_1 from 3.3×10^{-3} min^{-1} at pH 3.0 to 6.8×10^{-3} min^{-1} at pH 10.0 according to this trend. It is noteworthy that a similar pH-dependence has been reported by Wachter et al. [77] for the ECO degradation of CIP in a flow reactor equipped with a filter-press cell containing a BDD anode. The rise of CIP degradation at higher pH can be associated with the change of the ionic form of this antibiotic since it possesses two pK_a values of 6.09 and 8.62. At pH < 6.0 the cationic form of CIP (with a proton linked to the -NH- of the piperazine group) predominates in the medium, whereas at pH > 8.7 only the anionic form (with a lateral $-COO^-$ group) exists. The zwitterionic or neutral form (with $-NH_2^+-$ and $-COO^-$ group) is then present in the solution in the interval of pH 6.0-8.7. Since BDD(•OH) attacks much more rapidly the negative than positive compounds, the transition of pH from 3.0 to 10.0 favors the much

faster destruction of the more easily oxidizable anionic form of CIP hence strongly accelerating its degradation, as shows Fig. 5e.

The above results make evident that CIP is more largely removed by ECO with a BDD anode and in sulfate medium with increasing *j*, its concentration, and the solution pH, giving rise to a good performance with the novel pre-pilot batch plant. In these processes, the relative rate of the parasitic reactions of BDD(•OH) and the ionic form of the antibiotic present in solution played a key role to determine the positive action of such operating variables.

3.3. Influence of different aqueous matrices over CIP degradation

Once clarified the influence of the main operating variables in sulfate medium, the study of the oxidation power of the ECO process of CIP with a BDD anode using the new pre-pilot batch reactor was extended to aqueous matrices containing common species of natural waters and wastewaters such as Cl^- and CO_3^{2-} ions, as well as HA as representative of the natural organic matter.

Fig. 6a highlights the variation of the percent of CIP removal with time for 2 L of 10 mg L^{-1} antibiotic in different media with pure water at pH 7.0, 25 ºC, and j = 45 mA cm^{-2}. The aqueous matrices contained 0.050 M Na_2SO_4 (control) and 5 mM of Cl^-, CO_3^{2-}, or HA. As can be seen, the degradation was largely improved in the presence of Cl^- achieving 99.9% removal in only 180 min with a $k_1 = 1.20 \times 10^{-2}$ min^{-1}, a value much greater than 5.2×10^{-3} min^{-1} determined for the control test (see Table 2). The strong reactivity in the presence of this ion can be associated to the production of high quantities of active chlorine (HClO) at pH 7.0 from its anodic oxidation via reactions (20) and (21) [78,79], which attacks more rapidly CIP in the solution bulk than BDD(•OH) in the vicinity of the BDD anode.

$$2Cl^- \rightarrow Cl_2 + 2e^- \quad (20)$$

$$Cl_2 + H_2O \rightarrow HClO + Cl^- + H^+ \quad (21)$$

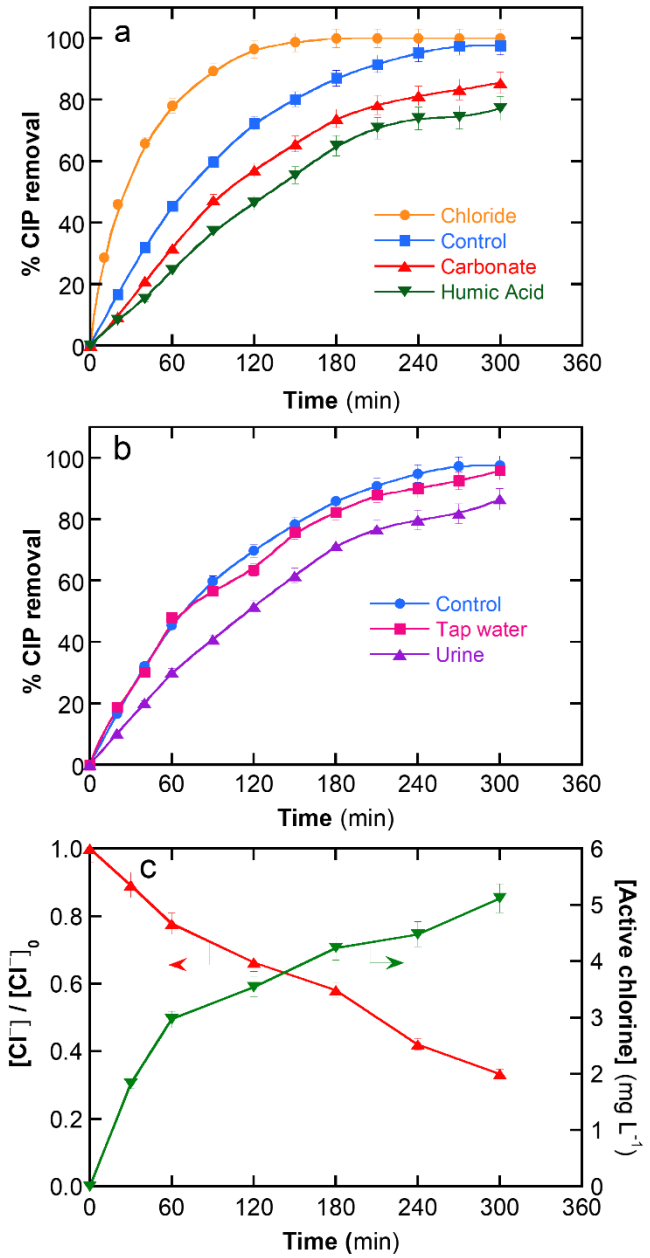

382

383 **Fig. 6.** Variation of the percentage of CIP removal with time for the electrochemical oxidation of 2
384 L of 10 mg L^{-1} CIP in different media at pH = 7.0 and 25 ºC using a pre-pilot batch BDD/stainless-
385 steel cell by applying a j = 45 mA cm^{-2}. Comparison of control conditions (0.050 M Na_2SO_4) with (a)
386 solutions with 5 mM of Cl^-, CO_3^{2-}, and humic acid (HA) and (b) tap water and synthetic urine as
387 aqueous matrices. (c) Change of normalized Cl^- concentration and active chlorine content with time
388 for the above assay with 5 mM Cl^-.

The opposite trend can be observed in Fig. 6a for the electrolytes containing CO_3^{2-} or HA, with slower removal than the control assay and lower k_1-values of 3.0×10^{-3} and 2.3×10^{-3} min^{-1}, respectively (Table 2). The inhibitory effect of CO_3^{2-} means that it acted as a scavenger of the generated BDD(•OH), consuming part of it and hence, decelerating the oxidation of the antibiotic[7,80] In contrast, HA as an organic compound was competitively oxidized with CIP by BDD(•OH). Consequently, in both cases, less BDD(•OH) was available for the antibiotic destruction.

From the above study, the degradation of CIP was carried out in more complex matrices like tap water and synthetic urine. Similar experimental conditions, i.e., 10 mg L^{-1} of spiked antibiotic, pH 7.0, and j = 45 mA cm^{-2}, were used and the results obtained are given in Fig. 6b. A slightly removal can be seen operating with tap water ($k_1 = 4.4 \times 10^{-3}$ min^{-1}) as compared with control conditions ($k_1 = 5.2 \times 10^{-3}$ min^{-1}) (see Table 2). This result allows inferring that despite the expected deceleration of CIP destruction by the competitive removal of the trace organic components of the tap water by BDD(•OH), the electrogeneration of oxidant HClO compensates the oxidative power loss, so the ECO practically maintains the oxidation power of ECO over the antibiotic abatement[81]. In contrast, the percent of CIP removal underwent a noticeable decrease in the synthetic urine matrix, yielding a k_1.value of 2.9×10^{-3} min^{-1}(see Table 2). In this case, the parallel oxidation of urea and uric acid by BDD(•OH) led to a strong decrease of the attack of this oxidant over CIP [82,83]

The good effectiveness of reaction (19) over the electroactive BDD anode and the subsequent quick formation of active chlorine by reaction (20) was confirmed by measuring the Cl^- abatement and the HClO production in the assay performed with 5 mM Cl^-. Fig. 6c illustrates a fast removal of 66.6% of the initial Cl^- (3.33 mM) in 300 min, whereas the active chlorine was continuously accumulated up to only 5.12 mg L^{-1} (0.10 mM). The very low content of HClO detected as compared to the high Cl^-concentration lost makes evident that most generated active chlorine reacted with CIP and its by-products causing its rapid destruction.

The above findings clearly demonstrate the large influence of the electrolytes and organic components of the solution over the ability of ECO to destroy CIP. The novel pre-pilot plant reactor with a BDD anode appropriately informs over such effects due to the good performance of BDD(•OH) and HClO generation under the experimental conditions tested.

3.4. Chemical oxygen demand abatement and by-products identification

The mineralization process is much slower than the degradation one because of the hard oxidation of some by-products formed like final short-linear aliphatic carboxylic acids, much more recalcitrant than the target molecule [63,84]. To confirm the continuous production of BDD(•OH) in the novel pre-pilot batch reactor and its power to remove organic pollutants, a longer experiment of 8 h was made by electrolyzing 2 L of 30 mg L^{-1} CIP (COD_0 = 190 mg L^{-1}) in 0.050 M Na_2SO_4 at pH = 7.0, 25 ºC, and j = 45 mA cm^{-2}. Fig. 7a highlights the progressive mineralization of the solution up to a final COD reduction near 94%, making evident the high oxidation power of the electrolytic system. Fig. 7b reveals a continuous fall of the percent of ACE from 14.3% to 5.0% as results of the gradual generation of more recalcitrant by-products. A very positive result was the constant EC_{COD} of 0.6±0.1 kWh (g COD)$^{-1}$ found during all the mineralization process, which confirms the good generation of BDD(•OH) in the powerful novel pre-pilot batch reactor tested.

The study of the above mineralization process was completed by quantifying the main by-products formed. Fig. 7c shows that the initial N of the 30 mg L^{-1} antibiotic solution was pre-eminently converted into nitrate (3.11 mg L^{-1} of N), and to much less extent into nitrite (0.029 mg L^{-1} of N) and ammonia (0.062 mg L^{-1} of N) after 300 min of electrolysis. This presupposes the release of 3.20 mg L^{-1} of N from the target molecule, accounting for the ionization of a 84% of the initial N (3.80 mg L^{-1}). This indicates either the destruction of the major part of N-derivatives or their total removal with a low generation of volatile N-compounds like N_xO_y gases, as usually described for N-aromatic compounds [34,85,86]

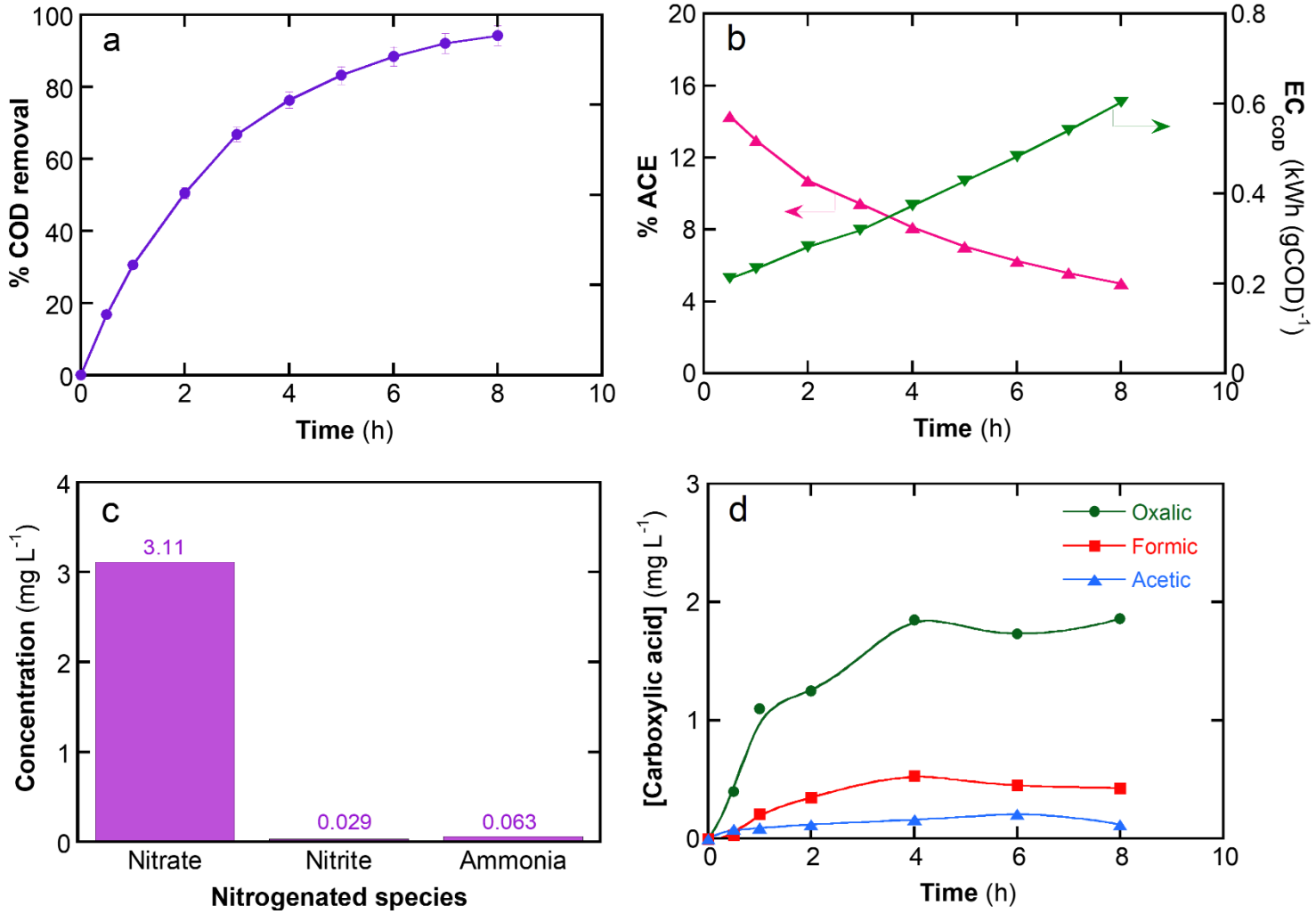

452 **Fig. 7.** Change of (a) the percentage of COD removal and (b) average current efficiency and the
453 energy consumption per unit COD mass with time for the electrochemical oxidation of 2 L of 30 mg
454 L^{-1} CIP (190 mg L^{-1} of initial COD) in 0.050 M Na_2SO_4 at pH = 7.0 and 25 ºC using a pre-pilot batch
455 BDD/stainless-steel cell at j = 45 mA cm^{-2}. (c) Concentration of nitrogenated species (in mg L^{-1} – N)
456 detected at 300 min of the above trial. (d) Time course of the concentration of generated carboxylic
457 acids.

458 The evolution of the main carboxylic acids generated in the mineralization process is depicted in
459 Fig. 7d. Low contents of acetic acid (< 0.16 mg L^{-1}) were detected during the 8 h electrolysis,
460 alongside greater concentrations of formic acid (approximately 0.5 mg L^{-1}) and preferentially oxalic
461 acid (1.86 mg L^{-1}). These acids are formed from the cleavage of the cyclic moieties of the antibiotic
462 and the two latter are directly mineralized to CO_2 [87,88]. The large stability of these acids in front
463 of BDD(•OH) explains the fact that CIP cannot be completely mineralized by ECO.

464 **4. Conclusions**

465 It has been shown the good performance of the novel pre-pilot batch reactor with a BDD anode
466 to generate physisorbed BDD(•OH) by ECO using turbulent flow simulation and secondary current
467 distribution modeling with a COMSOL Multiphysics software. This has been confirmed by studying
468 the removal of CIP under different experimental conditions. Faster degradation of this antibiotic was
469 found in sulfate medium by ECO at higher *j*, CIP concentration, and solution pH where BDD(•OH)
470 was the main oxidant. The action of such operating variables was determined by the relative rate of
471 the parasitic reactions of BDD(•OH) and the oxidation rate of the ionic form of the antibiotic present
472 in solution. Higher pH transformed its cationic form into its more easily oxidizable anionic form. The
473 degradation process was accelerated in chloride medium due to the additional generation of active
474 chlorine by Cl^- oxidation at the anode. It was confirmed that most of generated active chlorine reacted
475 with the antibiotic and its by-products. The presence of carbonate in the aqueous matrix caused an
476 inhibitory effect due to its scavenging action, whereas the addition of humic acid decelerated CIP
477 degradation by competitive oxidation with BDD(•OH). A decay in antibiotic abatement was also
478 found in tap water and synthetic urine by the electrolytes and organic compounds contained in them.
479 In sulfate medium, an almost total mineralization was achieved at long electrolysis time with
480 formation of recalcitrant acetic, oxalic, and formic acids. A final EC_{COD} = 0.6±0.1 kWh (g COD)$^{-1}$
481 was obtained during all the mineralization process demonstrating the good performance of the pre-

pilot batch reactor. The initial N of CIP was pre-eminently released as nitrate ion, and to lesser extent, as nitrite and ammonia.

Acknowledgments

This work was partially funded by São Paulo research foundation (grant #2014/50945-4, #2017/10118-0, #2019/20634-0 e #2021/08701-4) and National Council for Scientific, Technological Development (grant #303759/2014-3 and #303943/2021-1) and National Science Foundation (EEC-1449500) Nanosystems Engineering Research Center on Nanotechnology-Enabled Water Treatment.

References

[1] V. Lázár, A. Martins, R. Spohn, L. Daruka, G. Grézal, G. Fekete, M. Számel, P.K. Jangir, B. Kintses, B. Csörgő, Á. Nyerges, Á. Györkei, A. Kincses, A. Dér, F.R. Walter, M.A. Deli, E. Urbán, Z. Hegedűs, G. Olajos, O. Méhi, B. Bálint, I. Nagy, T.A. Martinek, B. Papp, C. Pál, Antibiotic-resistant bacteria show widespread collateral sensitivity to antimicrobial peptides, Nat. Microbiol. 3 (2018) 718–731. https://doi.org/10.1038/s41564-018-0164-0.

[2] M.A. Cook, G.D. Wright, The past, present, and future of antibiotics, Sci. Transl. Med. 14 (2022). https://doi.org/10.1126/scitranslmed.abo7793.

[3] N. Li, S. Tang, Y. Rao, J. Qi, Q. Zhang, D. Yuan, Peroxymonosulfate enhanced antibiotic removal and synchronous electricity generation in a photocatalytic fuel cell, Electrochim. Acta 298 (2019) 59–69. https://doi.org/10.1016/j.electacta.2018.12.063.

[4] Y. Hong, C. Li, G. Zhang, Y. Meng, B. Yin, Y. Zhao, W. Shi, Efficient and stable Nb_2O_5 modified g-C_3N_4 photocatalyst for removal of antibiotic pollutant, Chem. Eng. J. 299 (2016) 74–84. https://doi.org/10.1016/j.cej.2016.04.092.

503 [5] J.-Q. Xiong, M.B. Kurade, J.R. Kim, H.-S. Roh, B.-H. Jeon, Ciprofloxacin toxicity and its co-
504 metabolic removal by a freshwater microalga Chlamydomonas mexicana, J. Hazard. Mater.
505 323 (2017) 212–219. https://doi.org/10.1016/j.jhazmat.2016.04.073.
506 [6] L. Rizzo, C. Manaia, C. Merlin, T. Schwartz, C. Dagot, M.C. Ploy, I. Michael, D. Fatta-
507 Kassinos, Urban wastewater treatment plants as hotspots for antibiotic resistant bacteria and
508 genes spread into the environment: A review, Sci. Total Environ. 447 (2013) 345–360.
509 https://doi.org/10.1016/j.scitotenv.2013.01.032.
510 [7] A.J. dos Santos, G.V. Fortunato, M.S. Kronka, L.G. Vernasqui, N.G. Ferreira, M.R.V. Lanza,
511 Electrochemical oxidation of ciprofloxacin in different aqueous matrices using synthesized
512 boron-doped micro and nano-diamond anodes, Environ, Res. 204 (2022) 112027.
513 https://doi.org/10.1016/j.envres.2021.112027.
514 [8] Y. Jia, P. Wang, Y. Ou, Y. Yan, S. Zhou, L. Sun, H. Lu, Insights into the microbial response
515 mechanisms to ciprofloxacin during sulfur-mediated biological wastewater treatment using a
516 metagenomics approach, Water Res. 223 (2022) 118995.
517 https://doi.org/10.1016/j.watres.2022.118995.
518 [9] D. Palomares-Reyna, J.E. Carrera-Crespo, F.S. Sosa-Rodríguez, U.M. García-Pérez, I.
519 Fuentes-Camargo, L. Lartundo-Rojas, J. Vazquez-Arenas, Photo-electrochemical and
520 ozonation process to degrade ciprofloxacin in synthetic municipal wastewater, using C, N-
521 codoped TiO_2 with high visible-light absorption, J. Environ. Chem. Eng. 10 (2022) 107380.
522 https://doi.org/10.1016/j.jece.2022.107380.
523 [10] A. Hom-Diaz, Z.N. Norvill, P. Blánquez, T. Vicent, B. Guieysse, Ciprofloxacin removal
524 during secondary domestic wastewater treatment in high rate algal ponds, Chemosphere 180
525 (2017) 33–41. https://doi.org/10.1016/j.chemosphere.2017.03.125.

[11] K. Yi, D. Wang, QiYang, X. Li, H. Chen, J. Sun, H. An, L. Wang, Y. Deng, J. Liu, G. Zeng, Effect of ciprofloxacin on biological nitrogen and phosphorus removal from wastewater, Sci. Total Environ. 605–606 (2017) 368–375. https://doi.org/10.1016/j.scitotenv.2017.06.215.

[12] S.M. Zainab, M. Junaid, N. Xu, R.N. Malik, Antibiotics and antibiotic resistant genes (ARGs) in groundwater: A global review on dissemination, sources, interactions, environmental and human health risks, Water Res. 187 (2020) 116455. https://doi.org/10.1016/j.watres.2020.116455.

[13] P. Zhao, F. Yu, R. Wang, Y. Ma, Y. Wu, Sodium alginate/graphene oxide hydrogel beads as permeable reactive barrier material for the remediation of ciprofloxacin-contaminated groundwater, Chemosphere 200 (2018) 612–620. https://doi.org/10.1016/j.chemosphere.2018.02.157.

[14] S. Wu, P. Hua, D. Gui, J. Zhang, G. Ying, P. Krebs, Occurrences, transport drivers, and risk assessments of antibiotics in typical oasis surface and groundwater, Water Res. 225 (2022) 119138. https://doi.org/10.1016/j.watres.2022.119138.

[15] F. Huang, Z. An, M.J. Moran, F. Liu, Recognition of typical antibiotic residues in environmental media related to groundwater in China (2009−2019), J. Hazard. Mater. 399 (2020) 122813. https://doi.org/10.1016/j.jhazmat.2020.122813.

[16] L. Huang, Y. Mo, Z. Wu, S. Rad, X. Song, H. Zeng, S. Bashir, B. Kang, Z. Chen, Occurrence, distribution, and health risk assessment of quinolone antibiotics in water, sediment, and fish species of Qingshitan reservoir, South China, Sci. Rep. 10 (2020) 15777. https://doi.org/10.1038/s41598-020-72324-9.

[17] A.J. Watkinson, E.J. Murby, S.D. Costanzo, Removal of antibiotics in conventional and advanced wastewater treatment: Implications for environmental discharge and wastewater recycling, Water Res. 41 (2007) 4164–4176. https://doi.org/10.1016/j.watres.2007.04.005.

[18] V. Figueira, I. Vaz-Moreira, M. Silva, C.M. Manaia, Diversity and antibiotic resistance of Aeromonas spp. in drinking and waste water treatment plants, Water Res. 45 (2011) 5599–5611. https://doi.org/10.1016/j.watres.2011.08.021.

[19] H. Wang, Y. Shen, C. Hu, X. Xing, D. Zhao, Sulfadiazine/ciprofloxacin promote opportunistic pathogens occurrence in bulk water of drinking water distribution systems, Environ. Pollut. 234 (2018) 71–78. https://doi.org/10.1016/j.envpol.2017.11.050.

[20] S. Jia, P. Shi, Q. Hu, B. Li, T. Zhang, X.-X. Zhang, Bacterial community shift drives antibiotic resistance promotion during drinking water chlorination, Environ Sci. Technol. 49 (2015) 12271–12279. https://doi.org/10.1021/acs.est.5b03521.

[21] H. Wang, C. Hu, Y. Shen, B. Shi, D. Zhao, X. Xing, Response of microorganisms in biofilm to sulfadiazine and ciprofloxacin in drinking water distribution systems, Chemosphere 218 (2019) 197–204. https://doi.org/10.1016/j.chemosphere.2018.11.106.

[22] C. Xi, Y. Zhang, C.F. Marrs, W. Ye, C. Simon, B. Foxman, J. Nriagu, Prevalence of antibiotic resistance in drinking water treatment and distribution systems, Appl. Environ. Microbiol. 75 (2009) 5714–5718. https://doi.org/10.1128/AEM.00382-09.

[23] M. Bizi, F.E. el Bachra, Evaluation of the ciprofloxacin adsorption capacity of common industrial minerals and application to tap water treatment, Powder Technol. 362 (2020) 323–333. https://doi.org/10.1016/j.powtec.2019.11.047.

[24] T. aus der Beek, F.-A. Weber, A. Bergmann, S. Hickmann, I. Ebert, A. Hein, A. Küster, Pharmaceuticals in the environment-Global occurrences and perspectives, Environ. Toxicol. Chem. 35 (2016) 823–835. https://doi.org/10.1002/etc.3339.

[25] Yiruhan, Q.-J. Wang, C.-H. Mo, Y.-W. Li, P. Gao, Y.-P. Tai, Y. Zhang, Z.-L. Ruan, J.-W. Xu, Determination of four fluoroquinolone antibiotics in tap water in Guangzhou and Macao, Environ. Pollut. 158 (2010) 2350–2358. https://doi.org/10.1016/j.envpol.2010.03.019.

574 [26] H. Liu, Y. Gao, J. Wang, D. Ma, Y. Wang, B. Gao, Q. Yue, X. Xu, The application of UV/O_3
575 process on ciprofloxacin wastewater containing high salinity: performance and its degradation
576 mechanism, Chemosphere 276 (2021) 130220.
577 https://doi.org/10.1016/j.chemosphere.2021.130220.
578 [27] D.G.J. Larsson, C. de Pedro, N. Paxeus, Effluent from drug manufactures contains extremely
579 high levels of pharmaceuticals, J. Hazard. Mater. 148 (2007) 751–755.
580 https://doi.org/10.1016/j.jhazmat.2007.07.008.
581 [28] X. Chang, M.T. Meyer, X. Liu, Q. Zhao, H. Chen, J. Chen, Z. Qiu, L. Yang, J. Cao, W. Shu,
582 Determination of antibiotics in sewage from hospitals, nursery and slaughter house,
583 wastewater treatment plant and source water in Chongqing region of Three Gorge Reservoir
584 in China, Environ. Pollut. 158 (2010) 1444–1450.
585 https://doi.org/10.1016/j.envpol.2009.12.034.
586 [29] S. Ahmadzadeh, A. Asadipour, M. Pournamdari, B. Behnam, H.R. Rahimi, M. Dolatabadi,
587 Removal of ciprofloxacin from hospital wastewater using electrocoagulation technique by
588 aluminum electrode: Optimization and modelling through response surface methodology,
589 Process Saf. Environ. Protect. 109 (2017) 538–547.
590 https://doi.org/10.1016/j.psep.2017.04.026.
591 [30] E.A. Serna-Galvis, F. Ferraro, J. Silva-Agredo, R.A. Torres-Palma, Degradation of highly
592 consumed fluoroquinolones, penicillins and cephalosporins in distilled water and simulated
593 hospital wastewater by UV254 and UV254/persulfate processes, Water Res. 122 (2017) 128–
594 138. https://doi.org/10.1016/j.watres.2017.05.065.
595 [31] S. Ahmadzadeh, A. Asadipour, M. Pournamdari, B. Behnam, H.R. Rahimi, M. Dolatabadi,
596 Removal of ciprofloxacin from hospital wastewater using electrocoagulation technique by
597 aluminum electrode: optimization and modelling through response surface methodology,

598 Process Saf. Environ. Protect. 109 (2017) 538–547.
599 https://doi.org/10.1016/j.psep.2017.04.026.
600 [32] F. Yu, S. Sun, S. Han, J. Zheng, J. Ma, Adsorption removal of ciprofloxacin by multi-walled
601 carbon nanotubes with different oxygen contents from aqueous solutions, Chem. Eng. J. 285
602 (2016) 588–595. https://doi.org/10.1016/j.cej.2015.10.039.
603 [33] Z. Xu, D. Zhao, J. Lu, J. Liu, G. Dao, B. Chen, B. Huang, X. Pan, Multiple roles of
604 nanomaterials along with their based nanotechnologies in the elimination and dissemination of
605 antibiotic resistance, Chem. Eng. J. 455 (2023) 140927.
606 https://doi.org/10.1016/j.cej.2022.140927.
607 [34] M.S. Kronka, G. v. Fortunato, L. Mira, A.J. dos Santos, M.R.V. Lanza, Using Au NPs
608 anchored on ZrO_2/carbon black toward more efficient H_2O_2 electrogeneration in flow-by
609 reactor for carbaryl removal in real wastewater, Chem. Eng. J. 452 (2023) 139598.
610 https://doi.org/10.1016/j.cej.2022.139598.
611 [35] R. Montenegro-Ayo, A.C. Barrios, I. Mondal, K. Bhagat, J.C. Morales-Gomero, M.
612 Abbaszadegan, P. Westerhoff, F. Perreault, S. Garcia-Segura, Portable point-of-use
613 photoelectrocatalytic device provides rapid water disinfection, Sci. Total Environ. 737 (2020)
614 140044. https://doi.org/10.1016/j.scitotenv.2020.140044.
615 [36] A.J. dos Santos, H.L. Barazorda-Ccahuana, G. Caballero-Manrique, Y. Chérémond, P.J.
616 Espinoza-Montero, J.R. González-Rodríguez, U.J. Jáuregui-Haza, M.R. v. Lanza, A. Nájera,
617 C. Oporto, A. Pérez Parada, T. Pérez, V.D. Quezada, V. Rojas, V. Sosa, A. Thiam, R.A. Torres-
618 Palma, R. Vargas, S. Garcia-Segura, Accelerating innovative water treatment in Latin
619 America, Nat. Sustain. (2023). https://doi.org/10.1038/s41893-022-01042-z.
620 [37] S. Garcia-Segura, J.D. Ocon, M.N. Chong, Electrochemical oxidation remediation of real
621 wastewater effluents — A review, Process Saf. Environ. Prot. 113 (2018) 48–67.
622 https://doi.org/10.1016/j.psep.2017.09.014.

[38] L.R.D. Brito, S.O. Ganiyu, E. v. dos Santos, M.A. Oturan, C.A. Martínez-Huitle, Removal of antibiotic rifampicin from aqueous media by advanced electrochemical oxidation: role of electrode materials, electrolytes and real water matrices, Electrochim. Acta 396 (2021) 139254. https://doi.org/10.1016/j.electacta.2021.139254.

[39] J. Zhang, Y. Zhou, B. Yao, J. Yang, D. Zhi, Current progress in electrochemical anodic-oxidation of pharmaceuticals: mechanisms, influencing factors, and new technique, J. Hazard. Mater. 418 (2021) 126313. https://doi.org/10.1016/j.jhazmat.2021.126313.

[40] E.G. Araújo, A.J. dos Santos, D.R. da Silva, R. Salazar, C.A. Martínez-Huitle, Cysteic acid-modified glassy carbon electrode for monitoring oxalic acid (OA) concentration during its electrochemical oxidation at Ti/Pt anode, Electroanalysis 26 (2014) 748–755. https://doi.org/10.1002/elan.201300566.

[41] E. Brillas, Recent development of electrochemical advanced oxidation of herbicides. A review on its application to wastewater treatment and soil remediation, J. Clean. Prod. 290 (2021) 125841. https://doi.org/10.1016/j.jclepro.2021.125841.

[42] A.J. dos Santos, M.D. de Lima, D.R. da Silva, S. Garcia-Segura, C.A. Martínez-Huitle, Influence of the water hardness on the performance of electro-Fenton approach: decolorization and mineralization of Eriochrome Black T, Electrochim. Acta 208 (2016) 156–163. https://doi.org/10.1016/j.electacta.2016.05.015.

[43] E. do Vale-Júnior, A.J. dos Santos, D.R. da Silva, A.S. Fajardo, C.A. Martínez-Huitle, Electrochemical technologies for detecting and degrading benzoquinone using diamond films, ChemElectroChem 6 (2019) 4383–4390. https://doi.org/10.1002/celc.201900541.

[44] S.O. Ganiyu, M. Gamal El-Din, Insight into in-situ radical and non-radical oxidative degradation of organic compounds in complex real matrix during electrooxidation with boron doped diamond electrode: A case study of oil sands process water treatment, Appl. Catal. B: Environ. 279 (2020) 119366. https://doi.org/10.1016/j.apcatb.2020.119366.

[45] C.A. Martínez-Huitle, M. Panizza, Electrochemical oxidation of organic pollutants for wastewater treatment, Curr. Opin. Electrochem. 11 (2018) 62–71. https://doi.org/10.1016/j.coelec.2018.07.010.

[46] M. Brienza, S. Garcia-Segura, Electrochemical oxidation of fipronil pesticide is effective under environmental relevant concentrations, Chemosphere 307 (2022) 135974. https://doi.org/10.1016/j.chemosphere.2022.135974.

[47] L.G. Vernasqui, A.J. dos Santos, G. V. Fortunato, M.S. Kronka, H.L. Barazorda-Ccahuana, A.S. Fajardo, N.G. Ferreira, M.R.V. Lanza, Highly porous seeding-free boron-doped ultrananocrystalline diamond used as high-performance anode for electrochemical removal of carbaryl from water, Chemosphere 305 (2022) 135497. https://doi.org/10.1016/j.chemosphere.2022.135497.

[48] D. Clematis, M. Panizza, Application of boron-doped diamond electrodes for electrochemical oxidation of real wastewaters, Curr. Opin. Electrochem. 30 (2021) 100844. https://doi.org/10.1016/j.coelec.2021.100844.

[49] F. Sopaj, M.A. Rodrigo, N. Oturan, F.I. Podvorica, J. Pinson, M.A. Oturan, Influence of the anode materials on the electrochemical oxidation efficiency. Application to oxidative degradation of the pharmaceutical amoxicillin, Chem. Eng. J. 262 (2015) 286–294. https://doi.org/10.1016/j.cej.2014.09.100.

[50] E. do Vale-Júnior, D.R. da Silva, A.S. Fajardo, C.A. Martínez-Huitle, Treatment of an azo dye effluent by peroxi-coagulation and its comparison to traditional electrochemical advanced processes, Chemosphere 204 (2018) 548–555. https://doi.org/10.1016/j.chemosphere.2018.04.007.

[51] R. Stirling, W.S. Walker, P. Westerhoff, S. Garcia-Segura, Techno-economic analysis to identify key innovations required for electrochemical oxidation as point-of-use treatment

systems, Electrochim. Acta 338 (2020) 135874. https://doi.org/10.1016/j.electacta.2020.135874.

[52] S.O. Ganiyu, C.A. Martínez-Huitle, M.A. Rodrigo, Renewable energies driven electrochemical wastewater/soil decontamination technologies: a critical review of fundamental concepts and applications, Appl. Catal. B: Environ. 270 (2020) 118857. https://doi.org/10.1016/j.apcatb.2020.118857.

[53] Q. Yuan, S. Qu, R. Li, Z.-Y. Huo, Y. Gao, Y. Luo, Degradation of antibiotics by electrochemical advanced oxidation processes (EAOPs): performance, mechanisms, and perspectives, Sci. Total Environ. 856 (2023) 159092. https://doi.org/10.1016/j.scitotenv.2022.159092.

[54] H. Monteil, Y. Péchaud, N. Oturan, M.A. Oturan, A review on efficiency and cost effectiveness of electro- and bio-electro-Fenton processes: application to the treatment of pharmaceutical pollutants in water, Chem. Eng. J. 376 (2019) 119577. https://doi.org/10.1016/j.cej.2018.07.179.

[55] J. Xie, C. Zhang, T.D. Waite, Hydroxyl radicals in anodic oxidation systems: generation, identification and quantification, Water Res. 217 (2022) 118425. https://doi.org/10.1016/j.watres.2022.118425.

[56] C.A. Martínez-Huitle, M.A. Rodrigo, I. Sirés, O. Scialdone, Single and coupled electrochemical processes and reactors for the abatement of organic water pollutants: a critical review, Chem. Rev. 115 (2015) 13362–13407. https://doi.org/10.1021/acs.chemrev.5b00361.

[57] H. Monteil, Y. Pechaud, N. Oturan, C. Trellu, M.A. Oturan, Pilot scale continuous reactor for water treatment by electrochemical advanced oxidation processes: development of a new hydrodynamic/reactive combined model, Chem. Eng. J. 404 (2021) 127048. https://doi.org/10.1016/j.cej.2020.127048.

[58] S. Garcia-Segura, A.B. Nienhauser, A.S. Fajardo, R. Bansal, C.L. Conrad, J.D. Fortner, M. Marcos-Hernández, T. Rogers, D. Villagran, M.S. Wong, P. Westerhoff, Disparities between experimental and environmental conditions: research steps toward making electrochemical water treatment a reality, Curr. Opin. Electrochem. 22 (2020) 9–16. https://doi.org/10.1016/j.coelec.2020.03.001.

[59] A.J. dos Santos, P.L. Cabot, E. Brillas, I. Sirés, A comprehensive study on the electrochemical advanced oxidation of antihypertensive captopril in different cells and aqueous matrices, Appl. Catal. B: Environ. 277 (2020). https://doi.org/10.1016/j.apcatb.2020.119240.

[60] M.A. Sandoval, W. Calzadilla, R. Salazar, Influence of reactor design on the electrochemical oxidation and disinfection of wastewaters using boron-doped diamond electrodes, Curr. Opin. Electrochem. 33 (2022) 100939. https://doi.org/10.1016/j.coelec.2022.100939.

[61] O. Alrehaili, A.S. Fajardo, S. Garcia-Segura, P. Westerhoff, Microfluidic flow-by reactors minimize energy requirements of electrochemical water treatment without adding supporting electrolytes, Sep. Purif. Technol. 310 (2023) 123123. https://doi.org/10.1016/j.seppur.2023.123123.

[62] A.J.M. da Costa, M.S. Kronka, P.J.M. Cordeiro-Junior, G.V. Fortunato, A.J. dos Santos, M.R.V. Lanza, Treatment of tebuthiuron in synthetic and real wastewater using electrochemical flow-by reactor, J. Electroanal. Chem. 882 (2021) 224978. https://doi.org/10.1016/j.jelechem.2021.114978.

[63] A.J. dos Santos, S. Garcia-Segura, S. Dosta, I.G. Cano, C.A. Martínez-Huitle, E. Brillas, A ceramic electrode of ZrO_2-Y_2O_3 for the generation of oxidant species in anodic oxidation. Assessment of the treatment of Acid Blue 29 dye in sulfate and chloride media, Sep. Purif. Technol. 228 (2019) 115747. https://doi.org/10.1016/j.seppur.2019.115747.

[64] F.F. Rivera, T. Pérez, L.F. Castañeda, J.L. Nava, Mathematical modeling and simulation of electrochemical reactors: a critical review, Chem. Eng. Sci. 239 (2021) 116622. https://doi.org/10.1016/j.ces.2021.116622.

[65] T. Pérez, M.I. León, J.L. Nava, Numerical simulation of current distribution along the boron-doped diamond anode of a filter-press-type FM01-LC reactor during the oxidation of water, J. Electroanal. Chem. 707 (2013) 1–6. https://doi.org/10.1016/j.jelechem.2013.08.014.

[66] T. Pérez, L.F. Arenas, D. Villalobos-Lara, N. Zhou, S. Wang, F.C. Walsh, J.L. Nava, C.P. de León, Simulations of fluid flow, mass transport and current distribution in a parallel plate flow cell during nickel electrodeposition, J. Electroanal. Chem. 873 (2020) 114359. https://doi.org/10.1016/j.jelechem.2020.114359.

[67] H. Versteeg, W. Malalasekera, An Introduction to Computational Fluid Dynamics: The Finite Volume Method, 2st ed, UK, 2007.

[68] O.M. Cornejo, M.F. Murrieta, L.F. Castañeda, J.L. Nava, Characterization of the reaction environment in flow reactors fitted with BDD electrodes for use in electrochemical advanced oxidation processes: a critical review, Electrochim. Acta 331 (2020) 135373. https://doi.org/10.1016/j.electacta.2019.135373.

[69] J. Newman, K.E. Thomas-Alyea, Electrochemical Systems, 3rd ed., John Wiley & Sons, New Jersey, 2004.

[70] M. Panizza, G. Cerisola, Direct And mediated anodic oxidation of organic pollutants, Chem. Rev. 109 (2009) 6541–6569. https://doi.org/10.1021/cr9001319.

[71] B. Marselli, J. Garcia-Gomez, P.-A. Michaud, M.A. Rodrigo, Ch. Comninellis, Electrogeneration of hydroxyl radicals on boron-doped diamond electrodes, J. Electrochem. Soc. 150 (2003) D79. https://doi.org/10.1149/1.1553790.

742 [72] I. Sirés, E. Brillas, M.A. Oturan, M.A. Rodrigo, M. Panizza, Electrochemical advanced
743 oxidation processes: today and tomorrow. A review, Environ. Sci. Pollut. Res. 21 (2014) 8336–
744 8367. https://doi.org/10.1007/s11356-014-2783-1.
745 [73] A. Kapałka, G. Fóti, C. Comninellis, Kinetic modelling of the electrochemical mineralization
746 of organic pollutants for wastewater treatment, J. Appl. Electrochem. 38 (2007) 7–16.
747 https://doi.org/10.1007/s10800-007-9365-6.
748 [74] K.C. Araújo, E.V dos Santos, P.V Nidheesh, C.A. Martínez-Huitle, Fundamentals and
749 advances on the mechanisms of electrochemical generation of persulfate and sulfate radicals
750 in aqueous medium, Curr. Opin. Chem. Eng. 38 (2022) 100870.
751 https://doi.org/10.1016/j.coche.2022.100870.
752 [75] A.J. dos Santos, C.A. Martínez-Huitle, I. Sirés, E. Brillas, Use of Pt and boron-doped diamond
753 anodes in the electrochemical advanced oxidation of ponceau ss diazo dye in acidic sulfate
754 medium, ChemElectroChem. 5 (2018). https://doi.org/10.1002/celc.201701238.
755 [76] A.M. Sales Solano, C.K. Costa de Araújo, J. Vieira de Melo, J.M. Peralta-Hernandez, D.
756 Ribeiro da Silva, C.A. Martínez-Huitle, Decontamination of real textile industrial effluent by
757 strong oxidant species electrogenerated on diamond electrode: viability and disadvantages of
758 this electrochemical technology, Appl. Catal. B: Environ. 130–131 (2013) 112–120.
759 https://doi.org/10.1016/j.apcatb.2012.10.023.
760 [77] N. Wachter, J.M. Aquino, M. Denadai, J.C. Barreiro, A.J. Silva, Q.B. Cass, N. Bocchi, R.C.
761 Rocha-Filho, Electrochemical degradation of the antibiotic ciprofloxacin in a flow reactor
762 using distinct BDD anodes: Reaction kinetics, identification and toxicity of the degradation
763 products, Chemosphere 234 (2019) 461–470.
764 https://doi.org/10.1016/j.chemosphere.2019.06.053.
765 [78] A.J. dos Santos, A.S. Fajardo, M.S. Kronka, S. Garcia-Segura, M.R.V. Lanza, Effect of
766 electrochemically-driven technologies on the treatment of endocrine disruptors in synthetic

and real urban wastewater, Electrochim. Acta 376 (2021) 138034. https://doi.org/10.1016/j.electacta.2021.138034.

[79] S.O. Ganiyu, C.A. Martínez-Huitle, Nature, mechanisms and reactivity of electrogenerated reactive species at thin-film boron-doped diamond (BDD) electrodes during electrochemical wastewater treatment, ChemElectroChem 6 (2019) 2379–2392. https://doi.org/10.1002/celc.201900159.

[80] B.P. Chaplin, The prospect of electrochemical technologies advancing worldwide water treatment, Acc. Chem. Res. 52 (2019) 596–604. https://doi.org/10.1021/acs.accounts.8b00611.

[81] D. Clematis, M. Panizza, Application of boron-doped diamond electrodes for electrochemical oxidation of real wastewaters, Curr. Opin. Electrochem. 30 (2021) 100844. https://doi.org/10.1016/j.coelec.2021.100844.

[82] A. Atrashkevich, A.S. Fajardo, P. Westerhoff, W.S. Walker, C.M. Sánchez-Sánchez, S. Garcia-Segura, Overcoming barriers for nitrate electrochemical reduction: By-passing water hardness, Water Res. 225 (2022) 119118. https://doi.org/ 10.1016/j.watres.2022.119118.

[83] S. Cotillas, E. Lacasa, C. Sáez, P. Cañizares, M.A. Rodrigo, Disinfection of urine by conductive-diamond electrochemical oxidation, Appl. Catal. B: Environ. 229 (2018) 63–70. https://doi.org/10.1016/j.apcatb.2018.02.013.

[84] A. Phetrak, P. Westerhoff, S. Garcia-Segura, Low energy electrochemical oxidation efficiently oxidizes a common textile dye used in Thailand, J. Electroanal. Chem. 871 (2020) 114301. https://doi.org/10.1016/j.jelechem.2020.114301.

[85] V.S. Antonin, M.C. Santos, S. Garcia-Segura, E. Brillas, Electrochemical incineration of the antibiotic ciprofloxacin in sulfate medium and synthetic urine matrix, Water Res. 83 (2015) 31–41. https://doi.org/10.1016/j.watres.2015.05.066.

[86] A. El-Ghenymy, P.L. Cabot, F. Centellas, J.A. Garrido, R.M. Rodríguez, C. Arias, E. Brillas, Electrochemical incineration of the antimicrobial sulfamethazine at a boron-doped diamond anode, Electrochim. Acta 90 (2013) 254–264. https://doi.org/10.1016/j.electacta.2012.11.125.

[87] S. Garcia-Segura, J.A. Garrido, R.M. Rodríguez, P.L. Cabot, F. Centellas, C. Arias, E. Brillas, Mineralization of flumequine in acidic medium by electro-Fenton and photoelectro-Fenton processes, Water Res. 46 (2012) 2067–2076. https://doi.org/10.1016/j.watres.2012.01.019.

[88] J.R. Steter, E. Brillas, I. Sirés, On the selection of the anode material for the electrochemical removal of methylparaben from different aqueous media, Electrochim. Acta 222 (2016) 1464–1474. https://doi.org/10.1016/j.electacta.2016.11.125.